

Ice-covered lakes of Tibetan Plateau as solar heat collectors

Georgiy B Kirillin¹, Lijuan Wen², and Tom Shatwell³

¹Leibniz-Institute for Freshwater Ecology and Inland Fisheries

²Northwest Institute of Eco-Environment and Resources, Chinese Academy of Sciences

³Helmholtz Centre for Environmental Research

November 22, 2022

Abstract

The Qinghai-Tibet Plateau possesses the largest alpine lake system, which plays a crucial role in the land-atmosphere interaction. We report first observations on the thermal and radiation regime under ice of the largest freshwater lake of the Plateau. The results reveal that freshwater lakes on the Tibetan Plateau fully mix under ice. Due to strong solar heating, water temperatures increase above the maximum density value 1-2 months before the ice break, forming stable thermal stratification with subsurface temperatures $>6^\circ\text{C}$. The resulting heat flow from water to ice makes a crucial contribution to ice cover melt. After the ice breakup, the accumulated heat is released into the atmosphere during 1-2 days, increasing lake-atmosphere heat fluxes up to 500 W m^{-2} . The direct biogeochemical consequences of the deep convective mixing are aeration of the deep lake waters and upward supply of nutrients to the upper photic layer.

1 Ice-covered lakes of Tibetan Plateau as solar heat collectors

2 G. B. Kirillin¹, T. Shatwell², L. Wen³

3 ¹Department of Ecohydrology, Leibniz-Institute of Freshwater Ecology and Inland Fisheries (IGB), Berlin,
4 Germany

5 ²Department of Lake Research, Helmholtz Centre for Environmental Research - UFZ, Magdeburg,
6 Germany

7 ³Key Laboratory of Land Surface Process and Climate Change in Cold and Arid Region, Northwest
8 Institute of Eco-Environment and Resources, Chinese Academy of Sciences, Lanzhou, China

9 Key Points:

- 10 • An abnormal thermal regime under the ice cover of Tibetan lakes is revealed
11 • The lakes get heated above their maximum density temperature by extremely
12 high level of solar radiation penetrating the ice cover
13 • The stored heat shortens the ice-covered period and is quickly released into
14 the atmosphere after ice-off, affecting local climate

Abstract

The Qinghai-Tibet Plateau possesses the largest alpine lake system, which plays a crucial role in the land-atmosphere interaction. We report first observations on the thermal and radiation regime under ice of the largest freshwater lake of the Plateau. The results reveal that freshwater lakes on the Tibetan Plateau fully mix under ice. Due to strong solar heating, water temperatures increase above the maximum density value 1-2 months before the ice break, forming stable thermal stratification with subsurface temperatures > 6 °C. The resulting heat flow from water to ice makes a crucial contribution to ice cover melt. After the ice breakup, the accumulated heat is released into the atmosphere during 1-2 days, increasing lake-atmosphere heat fluxes up to 500 W m^{-2} . The direct biogeochemical consequences of the deep convective mixing are aeration of the deep lake waters and upward supply of nutrients to the upper photic layer.

1 Introduction

Nicknamed the “third pole”, the Plateau of Tibet is the world’s largest and highest plateau. It plays a crucial role in the earth’s climate and water cycle, for instance in the formation of the Asian monsoon system and as the origin of great Asian rivers such as the Yellow, Yangtze, Mekong, Salween, Brahmaputra, and Indus Rivers [Su et al., 2016]. The Tibetan Plateau is dotted with lakes, which are inherent components of the hydrological cycle driven by the “world’s largest water tower”.

Due to lack of regular monitoring, the physical regime of the Tibetan lakes remains largely unknown, making it difficult to estimate their contribution to regional-scale energy and mass exchange between land and the atmosphere. Observational data on the physical properties of Tibetan Plateau lakes are scarce and mostly confined to lake surface characteristics obtained by remote sensing [Lin et al., 2011; Zhang et al., 2014]. Moreover, air-lake fluxes measured using eddy covariance methods are too fragmentary to estimate the seasonal variations [Biermann et al., 2014; Li et al., 2015]. Especially little is known about heat transport within the lake water column, in particular, the thermal dynamics under ice. First reports on the mixing conditions and vertical heat transport in Tibetan lakes during the open water seasons were presented only recently [Wang et al., 2014; Wen et al., 2016; Kirillin et al., 2017; Huang et al., 2019], and the winter regime remains largely unexplored.

47 The lakes on the Tibetan Plateau are ice-covered for 4 to 5 months per year
48 [Kirillin et al., 2017]. The duration of ice cover is determined by heat redistribu-
49 tion in the sediment-water-ice system combined with lateral heat and salt inflows
50 and short-wave radiation under ice. The density stratification created by heat and
51 salt flows under ice can have lasting effects on the subsequent open water season by
52 restricting heat exchange within the water column, and heat and mass exchange be-
53 tween lake and atmosphere. Lakes respond more strongly to global climatic trends
54 than land or oceans due to their high thermal inertia and small size. Accordingly,
55 ice cover and winter dynamics are very sensitive to small changes in the global heat
56 budget [Magnuson et al., 2000].

57 The importance of the ice covered period for seasonal lake dynamics was only
58 recognized in the last decade [Kirillin et al., 2012]. Modern regional climate mod-
59 els either highly simplify or completely neglect thermodynamics of ice-covered lakes.
60 This produces large errors in estimates of seasonal ice formation and thaw with con-
61 sequences for the entire regional heat and mass balance in the land-atmosphere sys-
62 tem. Development of more sophisticated lake models requires observational data on
63 the thermal regime under ice and its major drivers.

64 The interactions with the monsoon circulation and global hydrological cycle
65 cause the alpine lakes of the Tibetan Plateau to respond quickly to global changes.
66 Thus first insights into the winter regime of Tibetan lakes are particularly intriguing.
67 We measured the vertical temperature distribution and short-wave radiation flux
68 under ice of the largest freshwater lake of Tibet during the entire ice season of 2015-
69 2016. We observed anomalous warming of the lake water under ice. In the middle of
70 the ice season, warming produced strong convection, which evolved into stable ther-
71 mal stratification when the temperature exceeded the maximum freshwater density
72 value of ≈ 4 °C. This caused heat to accumulate in the bulk of the water column ac-
73 companied by strong mixing at the water-ice boundary. The thermal regime differs
74 radically from that in the majority of ice-covered lakes, where water temperatures
75 stay below the maximum density value for the largest part of the ice-covered period.

76 Below, we discuss the driving mechanisms of this specific thermal regime and
77 its importance for the dynamics of the lake system of Tibet.

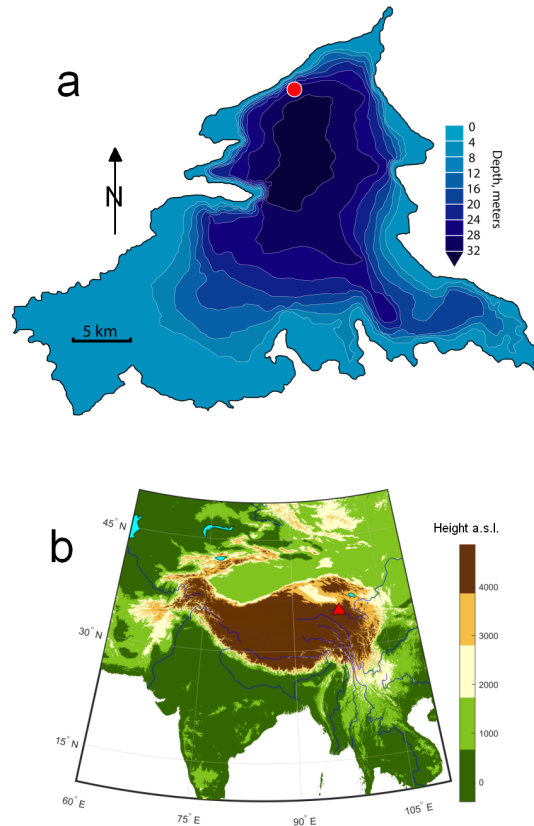
2 Materials and Methods

2.1 Study site

Ngoring Lake (Fig. 1) is the largest freshwater lake of Tibet (surface area 610 km²) located in the north-eastern part of the Plateau at 34.5-35.5° N and 97-98° E and belongs to the origin area of the Yellow River. The lake's altitude is ≈4300 m a.s.l., which counts it among the world's highest freshwater lakes. The mean and maximum depths are 17 and 32 m, respectively. Cold semi-arid continental climate prevails in the lake basin, the long-term (1953-2012) monthly mean air temperature varies from 7.7 °C in July to -16.2 °C in January, with an annual mean of -3.7 °C (Li et al., 2015). The lake is oligotrophic, i.e. presumably transparent for short-wave radiation, though according to the early observations of Przhevalsky [Пржевальский, 1888], the Yellow River inflow can produce strong variability in water transparency between the seasons, as well as between the different areas of the lake. The reported lake water transparency (Secchi depth) does not exceed 3 m (Kar 2014). The lake is ice-covered from early December to mid-April.

2.2 Measurements configuration

A chain with 18 RBR T-Solo temperature loggers (declared accuracy 0.002 °C) was moored in Ngoring Lake on 25 September 2015 at a site with depth of 26.2 m. The temperature loggers were suspended from a float at 1 m intervals to a depth of about 17 m and at 2-3 m intervals below. The uppermost logger was suspended 3.1 m beneath the water surface. During winter, ice thickness grows to more than 0.7 m according to modelling results [Kirillin et al., 2017] and own measurements. Accordingly, the uppermost temperature logger was at a depth of 2.4 m below the ice-water interface during the main winter period. Water temperatures were sampled at 0.1 Hz throughout the entire ice-covered period. Depth was monitored continuously with a pressure sensor at the lake bottom corrected for initial local air pressure. Downwelling short-wave radiation was measured at 10-minute intervals with two cosine-corrected photosynthetically active radiation (PAR, 400-700 nm) sensors (model DEFI2-L by JFE Advantech) moored at depths of 2.4 and 3.6 m, which corresponds to 1.8 and 3.0 m below the ice-water interface.



80 Figure 1. (A) Ngoring Lake bathymetry with location of the mooring station marked by
81 the red circle (B) geographical position of the lake (red triangle). The elevation data are from
82 GLOBE Task Team [1999].

2.3 Vertical heat fluxes

The spectrum of solar (wavelengths range 200-2500 nm) radiation is strongly modified by lake water, which absorbs the long-wave (infrared) part of the spectrum, while yellow substance absorbs the short-wave (ultraviolet) part. As a result, at < 1 m depth, > 95% of the transmitted radiation falls within the PAR spectral range of 400-700 nm [see e.g. Jerlov, 1976; Leppäranta et al., 2010]. Therefore, the measured PAR values at 2.4 and 3.6 m water depths were adopted as characteristic of the corresponding total downward short-wave radiation flux. We converted the measured quantum irradiance R_q [$\mu\text{mol s}^{-1} \text{m}^{-2}$] to the net downward short-wave radiation I_R [W m^{-2}] using the relationship obtained for ice-covered lakes $R_q/I_R = 4.6 \mu\text{mol J}^{-1}$ [see Leppäranta et al., 2010]; the corresponding measurement accuracy in the units of heat flux is $\pm 3 \text{ W m}^{-2}$. The light extinction coefficient γ and the radiation value at the ice-water interface I_0 were determined from a one-band exponential approximation of the short-wave radiation profile $I_R(z)$ in the water column,

$$I_R(z) = I_0 \exp(-\gamma z) \quad (1)$$

The light extinction coefficient was calculated using underwater radiation measurements between 10:00 hr and 14:00 hr.

The vertical “convective” heat flux within the bulk of the water column $Q_{conv}(z, t)$ as function of time t and depth z was estimated from temperatures measured by the thermistor chain $T(z, t)$ using the “flux-gradient method” which adopts the one-dimensional equation of heat transfer, neglecting horizontal advection:

$$C_p \rho \frac{\partial T(z, t)}{\partial t} = -\frac{\partial Q_{conv}(z, t)}{\partial z} - \frac{\partial I_R(z, t)}{\partial z}, \quad (2)$$

where $C_p \rho \approx 4.18 \cdot 10^6 \text{ J K}^{-1} \text{ m}^{-3}$ is the product of the water heat capacity and density. The solar radiation flux profile $I_R(z, t)$ was recovered from PAR measurements and Eq. (1). Integration of Eq. (2) from a reference depth H , usually chosen close to the lake bottom, to a depth z , and assuming negligible heat flux close to the lake bottom $Q_{conv}(H) \approx 0$, yields the expression

$$Q_{conv}(z, t) = I_R(H, t) - I_R(z, t) - C_p \rho \int_H^z \frac{\partial T(\zeta, t)}{\partial t} d\zeta, \quad (3)$$

which was solved numerically using finite differences for differentiation and the trapezoid method for integration. Q_{conv} in this formulation is the sum of all “non-radiative”

139 fluxes including buoyancy-driven convection, small-scale turbulence, and molecular
140 heat conduction.

141 2.4 Analytical model

142 In order to analyze the vertical heat transport by radiation and conduction in
143 an ice-covered lake with water temperatures higher than the temperature of maxi-
144 mum density of freshwater $T_m \approx 3.98$ °C, we applied the analytical solution of the
145 one-dimensional heat transfer equation derived by Kirillin and Terzhevik [2011]. The
146 conduction-radiation equation reads as

$$\frac{\partial T(z, t)}{\partial t} - \kappa \frac{\partial^2 T(z, t)}{\partial z^2} = -\frac{\partial}{\partial z} I_0 \exp(-\gamma z), \quad (4)$$

147 with the boundary conditions,

$$T(0, t) = 0, \quad T(\infty, t) = T_m, \quad T(z, 0) = \phi(z). \quad (5)$$

148 Here, I_0 is the radiation penetrating the ice normalized by the density and the spe-
149 cific heat of water; γ is the extinction coefficient, assumed to be uniform in the whole
150 daylight spectrum; $\kappa \approx 1.4 \cdot 10^{-7}$ m²s⁻¹ is the thermal diffusivity of water. The first
151 two boundary conditions in (5) are straightforward: the first fixes the temperature
152 of the ice-water interface at the freezing point, whereas the second expresses the fact
153 that the deeper parts of the water column are at the temperature of maximum den-
154 sity T_m and have been completely mixed by preceding convection. Due to the con-
155 vection the initial temperature profile $\phi(z)$ is homogeneous everywhere except for
156 the “conductive layer” (CL) under ice (red marked part of the temperature profile
157 in Fig. 4a). The temperature profile within the CL can be accurately reproduced by
158 the stationary form of the heat transfer equation, i.e. (4) without the first term on
159 the l.h.s. [Mironov et al., 2002]. Then, the initial profile $\phi(z) \equiv T(z, t)$, is given by

$$\begin{aligned} -\kappa \frac{d^2 \phi(z)}{dz^2} &= -\frac{d}{dz} I_0 \exp(-\gamma z) \quad \text{at } z \leq \delta, \\ \phi(z) &= T_m \quad \text{at } z > \delta, \end{aligned} \quad (6)$$

160 and the boundary conditions are

$$\phi(0) = 0, \quad \phi(z)(\delta) = T_m. \quad (7)$$

161 The solution of (6) is

$$\phi(z) = \begin{cases} \frac{I_0}{\kappa \gamma} (1 - e^{-\gamma z}) (1 - \frac{z}{\delta}) + T_m \frac{z}{\delta} & \text{at } 0 < z < \delta, \\ T_m & \text{at } z > \delta. \end{cases} \quad (8)$$

162 The thickness of the layer δ can be found from the additional condition $\partial T/\partial z = 0$
 163 at $z = \delta$. This leads to an algebraic equation for δ as function of the mixed layer
 164 temperature T_m , I_0 and γ [Barnes and Hobbie, 1960]

$$\kappa(T_m - T_f) + \delta I_0 e^{-\gamma\delta} + \gamma^{-1} I_0 (e^{-\gamma\delta} - 1) = 0 \quad (9)$$

The non-homogeneous heat transfer PDE problem (4) is closed through the conditions (8)-(9) and can be solved analytically, assuming the solar heat flux I_0 is constant in time. The final solution is

$$T(z, t) = \left\{ T_m - \frac{I_0}{\kappa\gamma} \right\} \left\{ \tilde{z} + \frac{1}{2} \left[\operatorname{erfc}_1(x) - \operatorname{erfc}_1(y) \right] \right\} \tilde{\delta}^{-1} + \frac{1}{2} \frac{I_0}{\kappa\gamma} \left\{ \tilde{\delta}^{-1} e^{-\gamma\delta} \left(\left[\operatorname{erf}(x) + \operatorname{erf}(y) \right] \tilde{z} + \left[e^{-x^2} - e^{-y^2} \right] \pi^{-1/2} \right) + e^{\tilde{\gamma}^2 - \gamma z} \operatorname{erfc}(y + \tilde{\gamma}) - e^{\tilde{\gamma}^2 + \gamma z} \operatorname{erfc}(x + \tilde{\gamma}) - 2e^{-\gamma z} + 2 \right\}, \quad (10)$$

165 where $\tilde{z} = z/\sqrt{4\kappa t}$, $\tilde{\delta} = \delta/\sqrt{4\kappa t}$, $\tilde{\gamma} = \gamma\sqrt{\kappa t}$,

166 $x = (\delta + z)/\sqrt{4\kappa t}$, $y = (\delta - z)/\sqrt{4\kappa t}$.

167 Here, erf, erfc and erfc_1 are the error function, the complimentary error function and
 168 the first order iterative complimentary error function, respectively [see e.g. Carslaw
 169 and Jaeger, 1959]. The derivative of eq. (10) with respect to z can be used to calcu-
 170 late the heat flux at the ice-water interface ($z = 0$), which is given by

$$\kappa \frac{\partial T(0, t)}{\partial z} = \frac{I_0}{\gamma\delta} \left\{ \gamma\delta e^{\gamma^2 t x} \operatorname{erf}\left(\frac{\delta + 2\gamma t x}{2\sqrt{t\kappa}}\right) - \gamma\delta e^{\gamma^2 t x} - \operatorname{erf}\left(\frac{\delta}{2\sqrt{t\kappa}}\right) + \operatorname{erf}\left(\frac{\delta}{2\sqrt{t\kappa}}\right) e^{-\gamma\delta} + \gamma\delta \right\} + \operatorname{erf}\left(\frac{\delta}{2\sqrt{t\kappa}}\right) \frac{\kappa T_m}{\delta} \quad (11)$$

171 3 Results

172 3.1 Surface cooling and ice formation

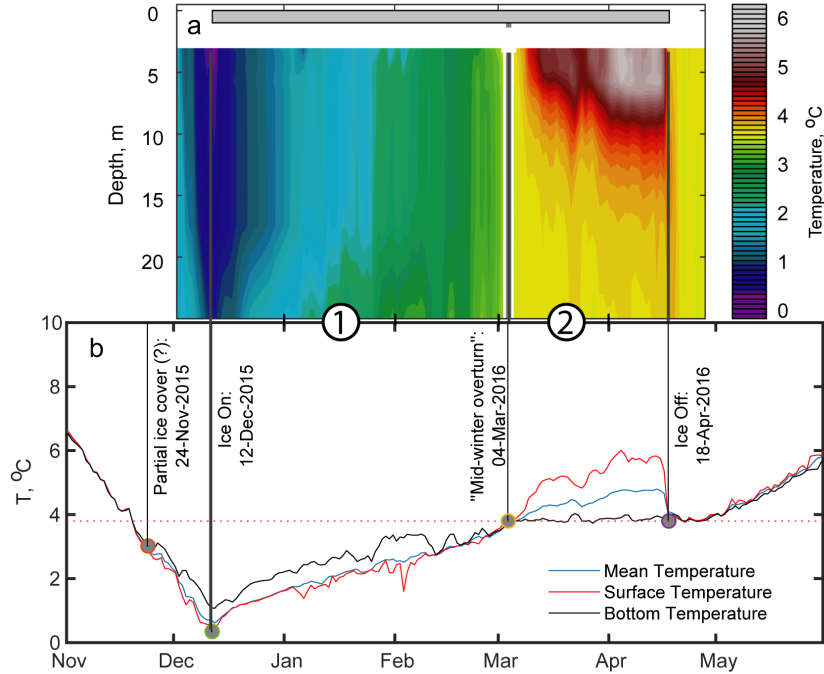
173 According to the water temperature data, the ice cover formed at the lake sur-
 174 face on 12 Dec \pm 1 day. Here, we used the evidence of the sudden drop in the latent
 175 and sensible heat release at the lake surface after the ice cover formation [Kirillin
 176 et al., 2012]. As a result, the water column quickly ceased cooling and the mean
 177 temperature began to rise when the entire lake surface froze (see the temperature

178 minimum at the “ice-on” mark in Fig. 2). Similarly, the moment of the “ice-off” was
179 identifiable in the water temperature data by a sudden drop of the mean water tem-
180 perature to the maximum density value T_m on 18 Apr (Fig. 2). The total ice-cover
181 duration was 126 days.

184 Prior to formation of the ice cover, cooling at the lake surface continued for
185 several weeks at a nearly constant rate of $0.2\text{ }^\circ\text{C day}^{-1}$, which corresponds to a net
186 heat loss from a 17 m deep lake of $> 150\text{ W m}^{-2}$. The water column started to
187 re-stratify around 24 Nov, when the water temperature dropped below T_m (Fig.2)
188 changing the sign of the surface buoyancy flux to positive and cancelling thereby
189 convection. However, at depths above the mean depth of the lake, the water column
190 remained nearly thermally homogeneous, indicating surface mixing by strong winds,
191 typical for the Tibetan Plateau, which destroy the near-surface stratification. As a
192 result, at the moment of ice formation, the entire 26 m deep water column cooled
193 down to $< 1\text{ }^\circ\text{C}$. Such a strong cooling rarely occurs in lowland freshwater lakes,
194 where stable stratification at temperatures below T_m develops near the lake surface
195 and decelerates the cooling of the bulk of the water column. It took only about 3
196 weeks for the surface temperature of the lake to cool from T_m to the freezing point
197 and the stable stratification at the begin of the ice-covered period did not exceed
198 $1\text{ }^\circ\text{C}$ over 20 m of the water column.

199 3.2 Convection by solar radiation at temperatures below T_m (“Normal winter”)

200 Because of the weak stratification at the moment of ice formation, a thermally-
201 homogeneous convective layer quickly developed driven by absorption of under-ice
202 solar radiation in the upper part of the water column. In early January, only 20 days
203 after the ice cover formation, the convective mixed layer achieved the mean depth
204 of the lake ($\sim 17\text{ m}$). Afterwards, the character of mixing changed: the gradual wa-
205 ter temperature increase was superimposed by irregular short-term oscillations with
206 characteristic time scales of a few days (Fig. 2). Heat intrusions at water depths be-
207 neath 17 m were clearly identifiable by repeated temperature increases of several
208 tenths of a Kelvin throughout January, with the strongest one lasting from 27 Jan
209 to 12 Feb (Fig. 2). The upper waters revealed in turn short-term temperature drops,
210 which were destroyed within 1-2 days by continuous heat supply from the solar ra-
211 diation absorption. After 12 Feb, 2 months after ice-on, free convection mixed the



182 Figure 2. Succession of mixing states in the ice-covered season of Ngoring Lake as revealed by
 183 the mean water temperature and its vertical gradient.

212 entire 26 m deep water column at the observational site, but several warm intrusions
 213 intermittently restored the near-bottom stratification. The temperature pattern is
 214 characteristic of advective heat transport from the warmer shallow littoral to the
 215 deep central part of the lake by downslope density currents with upwelling of colder
 216 water into the convective layer by transient residual currents [Kirillin et al., 2015].
 217 Eventually, on 04 Mar, the water column warmed up to T_m and was fully homoge-
 218 nized by convective mixing.

219 3.3 Strong heating and inverse stratification under ice (“Anomalous winter”)

220 As soon as the water temperature beneath the ice achieved T_m , the free convec-
 221 tion was halted, and stable vertical stratification developed in the bulk of the water
 222 column. Here, a distinct 3-layer vertical structure was created by the interplay of
 223 the volumetric heating by radiation absorption and the upward heat release at the
 224 ice base. The radiation absorption depresses convection and produces stable strati-
 225 fication with downward temperature decrease in the bulk of the water column, akin

226 to formation of the summer stratification. On the other hand, the heat release from
 227 the water column to the ice cover produces an upward decrease of the water temper-
 228 ature near the ice–water interface. This resulted in a subsurface temperature max-
 229 imum in the uppermost part of the water column covered by measurements, with
 230 temperatures growing continuously until the ice broke up in mid-April, when tem-
 231 perature values beneath the ice cover exceeded 6 °C (Fig. 2). The fixed temperature
 232 $T_f = 0\text{ °C}$ at the ice base requires a thermally stable interfacial layer with temper-
 233 atures increasing downwards from T_f and T_m to exist immediately under ice. This
 234 uppermost layer apparently did not exceed 1 m in thickness and was too thin to be
 235 covered by the moored sensors. The thermally unstable “inversion” layer with tem-
 236 peratures decreasing upwards from its maximum to T_m (see the schematic temper-
 237 ature profile Fig. 4b) was also not completely covered by the measurements. The
 238 modeling results (see below) and the temporal variability in the upper part of the
 239 measured temperature profiles suggest the thickness of the “inversion” layer to vary
 240 within 1-2 meters due to diurnal variations in solar radiation and the resulting con-
 241 vection.

242 Ice began to break up at midday on April 16 and had thawed completely within
 243 36 h. During this 36 h period, the temperature within the near-surface peak de-
 244 creased from 5.8 °C to 3.8 °C. The corresponding drop of the mean lake tempera-
 245 ture from 4.7 °C to 3.8 °C was equivalent to an average heat loss flux from the lake
 246 surface of up to 500 W m⁻².

247 3.4 Under-ice solar radiation

248 Underwater radiation measurements showed that the extinction coefficient $\gamma =$
 249 0.25 m⁻¹. Using the extinction coefficient and the Lambert-Beer law, we estimated
 250 the radiation at the ice-water interface from the measurements at the depth of the
 251 sensors. The mean downward radiation at the ice-water interface was 42.2 W m⁻²
 252 during the “normal” winter, and 46.5 W m⁻² during the “anomalous” winter. The
 253 mean solar radiation reaching the ice-surface during these periods was 171 and 280 W m⁻²,
 254 respectively, according to the ERA5 reanalysis [Hersbach et al., 2020]. Consider-
 255 ing that the visible band (400 - 700 nm) accounts for about 45% of broadband so-
 256 lar radiation on the Tibetan Plateau [Li et al., 2010], roughly 55% of visible radi-
 257 ation penetrated the ice cover during the normal winter, and about 37% during the

258 anomalous winter. This suggests little snow cover, especially during the earlier ice
 259 cover period, and an increase in light attenuation as the ice cover matured. Overall,
 260 this strong radiative warming suggests that all lakes on the Tibetan Plateau heat to
 261 above 4 °C during the ice-covered period.

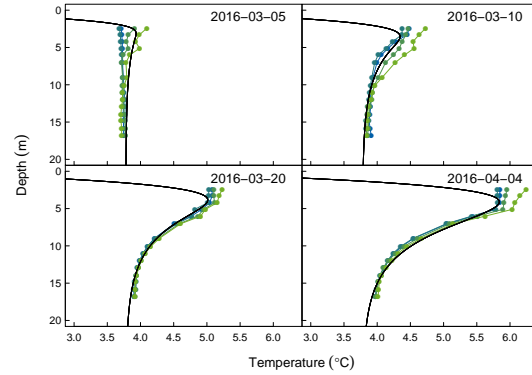
262 3.5 Modeling results

263 To analyze mixing conditions during the “anomalous winter” we fitted the model
 264 (10) using the measured solar radiation I_0 and extinction coefficient γ to the mea-
 265 sured temperature profiles and obtained the estimation of the thermal diffusivity
 266 under ice $\kappa = 1.41 \cdot 10^{-6} \pm 4.6 \cdot 10^{-8} \text{ m}^2 \text{ s}^{-1}$. The model described the observed
 267 daily mean temperatures well with a root mean square error of 0.19 °C and bias of
 268 0.012 °C (Fig. 3).

269 Since the radiation-diffusion model assumed a stationary radiation flux and
 270 neglected gravitational instability, it did not capture the diurnal temperature vari-
 271 ations and the development of the nearly homogeneous vertical temperature distri-
 272 bution in the upper part of the measured temperature profiles created by convective
 273 mixing in the “inversion” layer (Fig.3d). However, the model adequately reproduced
 274 both the strength of the subsurface temperature peak and the shape of the temper-
 275 ature profile in the stably stratified water column beneath, indicating the simple
 276 radiation-diffusion balance to hold true in the bulk of the water column. It is worth
 277 noting that the fitted value of the vertically-constant diffusion $\kappa = \mathcal{O}(10^{-6}) \text{ m}^2 \text{ s}^{-1}$ is
 278 an order of magnitude higher than the molecular value, suggesting additional mixing
 279 mechanisms contributed to the vertical heat transport, such as breaking of internal
 280 waves in the stably stratified water column. Using Eq. (11), the model suggested
 281 that the heat flux from the water to the ice was on average 22.3 W m^{-2} . In reality
 282 this heat flux can be much higher due to strong mixing under the ice caused by sec-
 283 ondary convection, which the model does not account for.

287 3.6 Heat budget

290 The critical differences in the heat budget of the lake water column for the
 291 “normal” and the “anomalous” winter are distinguishable in the mean profiles of the
 292 vertical heat flux during both periods (Fig. 4) calculated from Eq. (3). In the first

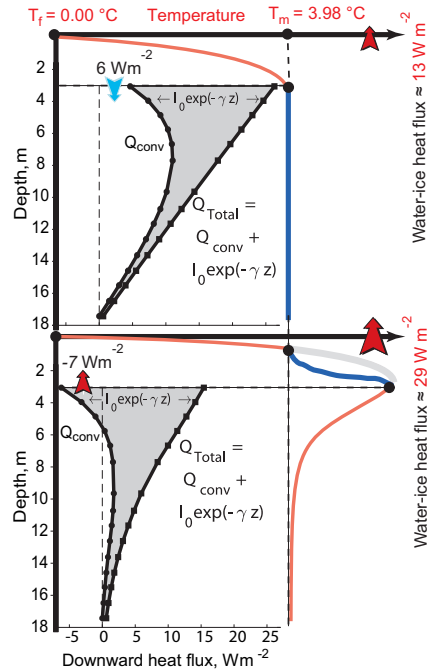


284 Figure 3. Modeled (black solid lines) and observed (lines with symbols) temperature profiles
 285 during the period of inverse stratification. The observed profiles are 4-hour averages on the given
 286 calendar day.

293 period, the profile of the total flux $Q_{conv} + I_R$ is linear, corresponding to the homo-
 294 geneous vertical temperature distribution produced by convective mixing. At the
 295 upper boundary of the water column covered by the measurements (water depth
 296 ≈ 3 m), the downward flux is around 6 W m^{-2} . Using this value as a boundary con-
 297 dition and taking into account the fixed temperature of 0°C at the ice-water inter-
 298 face, application of Eq. (3) to the layer 0–3 m yields the estimation of the mean flux
 299 at the ice base as $\approx -13 \text{ W m}^{-2}$. In the second period, after formation of the sta-
 300 ble density stratification, the downward heat flux dropped significantly in the bulk
 301 of the water column (Fig. 4b), and changed its sign to negative (upward) at 3–6 m
 302 water depth. The boundary value of -7 W m^{-2} at 3 m depth, when substituted to
 303 Eq. (3), results in the ice base heat flux of $\approx -29 \text{ W m}^{-2}$, which is about $1/3$ higher
 304 than the estimate obtained with the analytical model above.

305 4 Discussion

306 Our results elucidate novel aspects of the thermodynamics of alpine ice-covered
 307 lakes that are particularly relevant not only to their behavior as aquatic ecosystems,
 308 but also to the role that the world’s largest high-mountain lake system—the Qinghai-
 309 Tibetan Plateau—plays in the land-atmosphere interaction. The combined effect of
 310 strong solar radiation and the cold atmosphere produces cardinal differences between
 311 ice-covered Tibetan lakes and lowland high-latitude freshwaters in terms of the ther-
 312 mal and radiation regime.



288 Figure 4. Mean vertical heat fluxes (lines with dots) and schematic temperature profiles (solid
 289 lines) during (a) the convective period and (b) the stratified period.

313 The most striking feature of the observed thermal structure is the heating of
 314 the water column up to the maximum density value several weeks before the ice
 315 breakup. Early limnological studies [Rossolimo, 1929; Koźmiński and Wiszniewski,
 316 1934] reported the phenomenon of anomalous heating of ice-covered freshwater lakes
 317 up to temperatures exceeding T_m followed by a “temperature dichotomy” with a sub-
 318 surface temperature maximum. However, the situation was rather short-lived, ap-
 319 pearing just days before the ice breakup and resulting in strong acceleration of the
 320 ice cover melt [Mironov et al., 2002; Kirillin and Terzhevik, 2011].

321 Both high transparency of the oligotrophic lake water and dry thin atmosphere
 322 determine the particular role of the short-wave solar irradiance I_R in the heat bud-
 323 get of alpine lakes. The surface value of total (direct and diffuse) I_R at heights of the
 324 Tibetan Plateau is close the no-atmosphere values [Li et al., 2015, 2000]. As a result,
 325 a high amount of solar radiation penetrates the snow-free ice cover and is stored dis-
 326 tributed across the transparent water column. On the other hand, the strong heat
 327 loss from the ice surface prevents ice melt and release of the heat accumulated in
 328 the water back to the atmosphere. The strong surface heat loss also ensures low

329 heat content and weak stratification of the water column at the moment of ice-on
330 as compared to the non-alpine ice-covered lakes, where dense warm waters with tem-
331 peratures $\lesssim T_m$ typically accumulate near the lake bottom [Bengtsson and Svensson,
332 1996; Kirillin et al., 2012]. Weak thermal stratification additionally contributes to
333 the quick penetration of the convective mixing into the water column after the ice-
334 on: Lake Ngoring was mixed down to its mean depth within less than a month, and,
335 assuming the observed conditions as typical for freshwater Tibetan lakes, convection
336 would completely mix any lake with total depth of $\lesssim 100$ m during the 4 months of
337 the ice-covered period.

338 Another remarkable feature of convective mixing in Tibetan lakes indirectly ev-
339 idenced by our results is the strong horizontal heat exchange during the later stage
340 of the convective period. As soon as the mixed layer depth exceeds the mean lake
341 depth, a significant shallow part of the lake gets mixed by convection to the bot-
342 tom and starts to warm faster than the deeper pelagic areas, where the solar en-
343 ergy is fractionated between the mixed layer warming and convective entrainment
344 into the stratified water column. As a result, warm dense waters sink along the bot-
345 tom slope, increasing the thermal stratification in the central part of the lake and
346 contributing simultaneously to homogenization of the water column, as exemplified
347 by the temperatures observed in late February (Fig. 2). The effect has been pre-
348 viously reported at the concluding stage of the ice-covered period in high-latitude
349 lakes [Kirillin et al., 2015], but may contribute much more strongly to mixing of
350 alpine lakes due to the stronger solar heating and, as a result, higher lateral tem-
351 perature gradients lasting for a significant part of winter.

352 The “anomalous” winter with under-ice water temperatures exceeding the max-
353 imum density value lasts in Tibetan lakes for more than a month, or about one third
354 of the entire ice-covered period. Consequently, the thousands of lakes of the Qinghai-
355 Tibet Plateau act as “lenses” spotted around the landscape and accumulating solar
356 heat in a thin subsurface layer under ice. The heat stored under lake ice accelerates
357 the ice melt: our estimations of the water-ice heat flux of $10\text{-}30\text{ W m}^{-2}$ are about an
358 order of magnitude higher than estimates from temperate and polar lakes [Bengtsson
359 and Svensson, 1996; Jakkila et al., 2009; Kirillin et al., 2018]. Immediately after the
360 ice breakup, the heat is released to the atmosphere within 1-2 days, creating “hot
361 spots” in land-atmosphere interaction with strong upward heat fluxes of $\sim 500\text{ W m}^{-2}$,

362 which are several times higher than those from the surrounding land [Li et al., 2015;
363 Wen et al., 2016]. The resulting effects on the atmospheric boundary layer include
364 strong horizontal temperature differences, intensification of convection driven by sur-
365 face heat flux, and strong water mass flux into the atmosphere. Taking into account
366 the large lake-covered area of the Qinghai-Tibet Plateau and importance of its water
367 budget, the cumulative lake effect is regional or even global rather than local. It is
368 important to mention the potential biogeochemical and ecological projections of the
369 specific mixing and temperature regime. The full mixing by convection of the en-
370 tire water column in mid-winter ensures supply of the dissolved oxygen to the near-
371 bottom layers, suggesting the Tibetan lakes are much less prone to winter hypoxia
372 typical for small ice-covered lakes in higher latitudes [Golosov et al., 2007; Terzhevik
373 et al., 2009]. The high amount of subsurface radiation is in turn favorable for under-
374 ice plankton primary production, while relatively warm conditions in the subsurface
375 temperature maximum stimulate microbiological activity. Particularly the deep con-
376 vective mixing, which brings deep nutrients to the surface, followed by formation of
377 a shallow stably stratified layer with high light availability are precisely the condi-
378 tions that cause large phytoplankton blooms in lowland lakes [Kong et al., 2021].
379 Apart from contribution to the carbon and nutrients cycles, both the high radiation
380 and the warm subsurface temperature may stimulate oxic methane production [Tang
381 et al., 2016; Günthel et al., 2019] at levels significant to contribute to the greenhouse
382 gas emissions to the atmosphere.

383 5 Conclusions

384 Our findings suggest that all freshwater (and apparently the majority of brack-
385 ish) lakes on the Tibetan Plateau fully mix under ice, so that the convenient con-
386 cept of winter stagnation, as known from traditional lake science, is inapplicable for
387 these lakes. The 1-2 months long period of stable stratification at water tempera-
388 tures above the maximum density value is an exceptional feature of high-altitude
389 freshwaters. The resulting strong temperature gradient at the ice-water interface and
390 a thin unstable layer right beneath intensify the heat flow from water to ice, making
391 a crucial contribution to ice cover melting. The direct consequences of the deep con-
392 vective mixing are aeration of the deep lake waters and upward supply of nutrients

393 to the upper photic layer, both suggesting versatile biogeochemical and ecological
394 interactions specific for high-altitude lakes.

395 Acknowledgments

396 The study was a part of the research project “Lakes of Tibet as part of the Climate
397 System” (LaTiCS) funded by the Sino-German Center for Research Promotion (CDZ
398 project GZ1259) and by the German Research Foundation (DFG project KI 853/13-
399 1). GK was additionally supported by the DFG grant KI 853/16-1. The data pre-
400 sented in the study will be made available by acceptance via the IGB Freshwater
401 Research and Environmental Database (FRED) at <https://fred.igb-berlin.de/>

402 References

- 403 Barnes, D. F., and J. E. Hobbie (1960), Rate of melting at the bottom of floating
404 ice, *US Geol. Serv. Profess. Papers*, 400, B392–B394.
- 405 Bengtsson, L., and T. Svensson (1996), Thermal regime of ice covered swedish lakes,
406 *Hydrology Research*, 27(1-2), 39–56.
- 407 Biermann, T., W. Babel, W. Ma, X. Chen, E. Thiem, Y. Ma, and T. Foken (2014),
408 Turbulent flux observations and modelling over a shallow lake and a wet grass-
409 land in the Nam Co basin, Tibetan Plateau, *Theoretical and Applied Climatology*,
410 116(1-2), 301–316.
- 411 Carlslaw, H. S., and C. S. Jaeger (1959), *Conduction of Heat in Solids*, 2nd ed., Ox-
412 ford University Press, New York.
- 413 GLOBE Task Team (1999), *The Global Land One-kilometer Base El-
414 evation (GLOBE) Digital Elevation Model, Version 1.0.*, National
415 Oceanic and Atmospheric Administration, National Geophysical
416 Data Center, 325 Broadway, Boulder, Colorado 80305-3328, U.S.A.,
417 <http://www.ngdc.noaa.gov/mgg/topo/globe.html> accessed Mar 2021.
- 418 Golosov, S., O. Maher, E. Schipunova, A. Terzhevik, G. Zdrovennova, and G. Kir-
419 illin (2007), Physical background of the development of oxygen depletion in ice-
420 covered lakes, *Oecologia*, 151(2), 331–340.
- 421 Günthel, M., D. Donis, G. Kirillin, D. Ionescu, M. Bizic, D. F. McGinnis, H.-P.
422 Grossart, and K. W. Tang (2019), Contribution of oxic methane production to
423 surface methane emission in lakes and its global importance, *Nature communica-*

- 424 tions, 10(1), 1–10.
- 425 Hersbach, H., B. Bell, P. Berrisford, S. Hirahara, A. Horányi, J. Muñoz-Sabater,
426 J. Nicolas, C. Peubey, R. Radu, D. Schepers, et al. (2020), The era5 global reanal-
427 ysis, *Quarterly Journal of the Royal Meteorological Society*, 146(730), 1999–2049.
- 428 Huang, W., J. Zhang, M. Leppäranta, Z. Li, B. Cheng, and Z. Lin (2019), Thermal
429 structure and water-ice heat transfer in a shallow ice-covered thermokarst lake in
430 central qinghai-tibet plateau, *Journal of Hydrology*, 578, 124,122.
- 431 Jakkila, J., M. Leppäranta, T. Kawamura, K. Shirasawa, and K. Salonen (2009),
432 Radiation transfer and heat budget during the ice season in lake pääjärvi, finland,
433 *Aquatic Ecology*, 43(3), 681–692.
- 434 Jerlov, N. G. (1976), *Marine optics*, Elsevier Oceanography Series 14, Elsevier,
435 Amsterdam-Oxford-New York.
- 436 Kirillin, G., and A. Terzhevik (2011), Thermal instability in freshwater lakes under
437 ice: Effect of salt gradients or solar radiation?, *Cold Regions Science and Technol-*
438 *ogy*, 65(2), 184–190.
- 439 Kirillin, G., M. Leppäranta, A. Terzhevik, N. Granin, J. Bernhardt, C. Engelhardt,
440 T. Efremova, S. Golosov, N. Palshin, P. Sherstyankin, G. Zdorovenнова, and
441 R. Zdorovennov (2012), Physics of seasonally ice-covered lakes: a review, *Aquatic*
442 *Sciences*, 74(4), 659–682, doi:10.1007/s00027-012-0279-y.
- 443 Kirillin, G., A. Forrest, K. Graves, A. Fischer, C. Engelhardt, and B. Laval (2015),
444 Axisymmetric circulation driven by marginal heating in ice-covered lakes, *Geo-*
445 *physical Research Letters*, 42(8), 2893–2900.
- 446 Kirillin, G., L. Wen, and T. Shatwell (2017), Seasonal thermal regime and climatic
447 trends in lakes of the tibetan highlands, *Hydrology and Earth System Sciences*,
448 21(4), 1895–1909.
- 449 Kirillin, G., I. Aslamov, M. Leppäranta, and E. Lindgren (2018), Turbulent mixing
450 and heat fluxes under lake ice: the role of seiche oscillations, *Hydrology and Earth*
451 *System Sciences*, 22(12), 6493–6504.
- 452 Kong, X., M. Seewald, T. Dadi, K. Friese, C. Mi, B. Boehrer, M. Schultze, K. Rinke,
453 and T. Shatwell (2021), Unravelling winter diatom blooms in temperate lakes us-
454 ing high frequency data and ecological modeling, *Water Research*, 190, 116,681.
- 455 Koźmiński, Z., and J. Wiszniewski (1934), Über die Vorfrühlingthermik der Wigry-
456 Seen, *Archiv f. Hydrobiol.*, 28, 198–235.

- 457 Leppäranta, M., A. Terzhevik, and K. Shirasawa (2010), Solar radiation and ice
458 melting in Lake Vendyurskoe, Russian Karelia, *Hydrology Research*, 41(1), 50–62.
- 459 Li, C., Y. Gong, T. Duan, Y. Zhu, L. Chen, and W. Li (2000), Observational
460 study of super solar constant of the solar radiation over qinghai-tibet plateau, *J.*
461 *Chengdu Institute Meteorol*, 15(2), 107–112.
- 462 Li, R., L. Zhao, Y. Ding, S. Wang, G. Ji, Y. Xiao, G. Liu, and L. Sun (2010),
463 Monthly ratios of par to global solar radiation measured at northern tibetan
464 plateau, china, *Solar Energy*, 84(6), 964–973.
- 465 Li, Z., S. Lyu, Y. Ao, L. Wen, L. Zhao, and S. Wang (2015), Long-term energy flux
466 and radiation balance observations over Lake Ngoring, Tibetan Plateau, *Atmo-*
467 *spheric Research*, 155, 13–25.
- 468 Lin, Z., F. Niu, H. Liu, and J. Lu (2011), Hydrothermal processes of alpine tundra
469 lakes, Beiluhe basin, Qinghai-Tibet Plateau, *Cold Regions Science and Technol-*
470 *ogy*, 65(3), 446–455.
- 471 Magnuson, J. J., D. M. Robertson, B. J. Benson, R. H. Wynne, D. M. Livingstone,
472 T. Arai, R. A. Assel, R. G. Barry, V. Card, E. Kuusisto, et al. (2000), Historical
473 trends in lake and river ice cover in the northern hemisphere, *Science*, 289(5485),
474 1743–1746.
- 475 Mironov, D., A. Terzhevik, G. Kirillin, T. Jonas, J. Malm, and D. Farmer (2002),
476 Radiatively driven convection in ice-covered lakes: Observations, scaling, and a
477 mixed layer model, *Journal of Geophysical Research: Oceans*, 107(C4).
- 478 Rossolimo, L. L. (1929), *Thermik der Kossino-Seen*, *Trudy Kos. Biol. Stancii*, 10,
479 3–49, (in Russian with German resume).
- 480 Su, F., L. Zhang, T. Ou, D. Chen, T. Yao, K. Tong, and Y. Qi (2016), Hy-
481 drological response to future climate changes for the major upstream river
482 basins in the Tibetan Plateau, *Global and Planetary Change*, 136, 82–95, doi:
483 10.1016/j.gloplacha.2015.10.012.
- 484 Tang, K. W., D. F. McGinnis, D. Ionescu, and H.-P. Grossart (2016), Methane pro-
485 duction in oxic lake waters potentially increases aquatic methane flux to air, *Envi-*
486 *ronmental Science & Technology Letters*, 3(6), 227–233.
- 487 Terzhevik, A., S. Golosov, N. Palshin, A. Mitrokhov, R. Zdrovennov, G. Zdroven-
488 nova, G. Kirillin, E. Shipunova, and I. Zverev (2009), Some features of the
489 thermal and dissolved oxygen structure in boreal, shallow ice-covered lake

- 490 vendyurskoe, russia, *Aquatic Ecology*, 43(3), 617–627.
- 491 Wang, M., J. Hou, and Y. Lei (2014), Classification of Tibetan lakes based on varia-
492 tions in seasonal lake water temperature, *Chinese Science Bulletin*, 59(34), 4847–
493 4855, doi:10.1007/s11434-014-0588-8.
- 494 Wen, L., S. Lyu, G. Kirillin, Z. Li, and L. Zhao (2016), Air-lake boundary layer and
495 performance of a simple lake parameterization scheme over the Tibetan highlands,
496 *Tellus A*, 68(0), doi:10.3402/tellusa.v68.31091.
- 497 Zhang, G., T. Yao, H. Xie, J. Qin, Q. Ye, Y. Dai, and R. Guo (2014), Estimating
498 surface temperature changes of lakes in the Tibetan Plateau using MODIS LST
499 data, *Journal of Geophysical Research: Atmospheres*, 119(14), 8552–8567.
- 500 Пржевальский, Н. (1888), От Кяхты на истоки Желтой реки, исследование
501 северной окраины Тибета и путь через Лоб-Нор по бассейну Тарима., 1 ed.,
502 Издание Имп. Русского Географического Общества, Санкт-Петербург.

Figure 1.

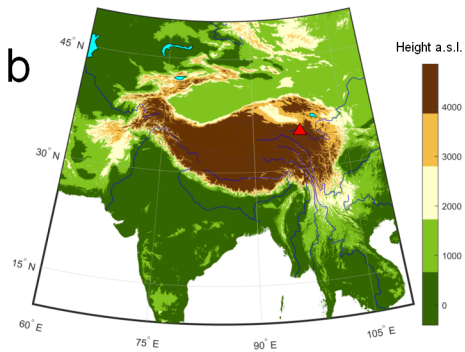
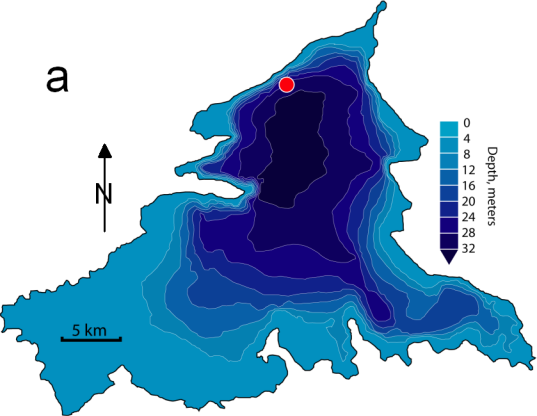


Figure 2.

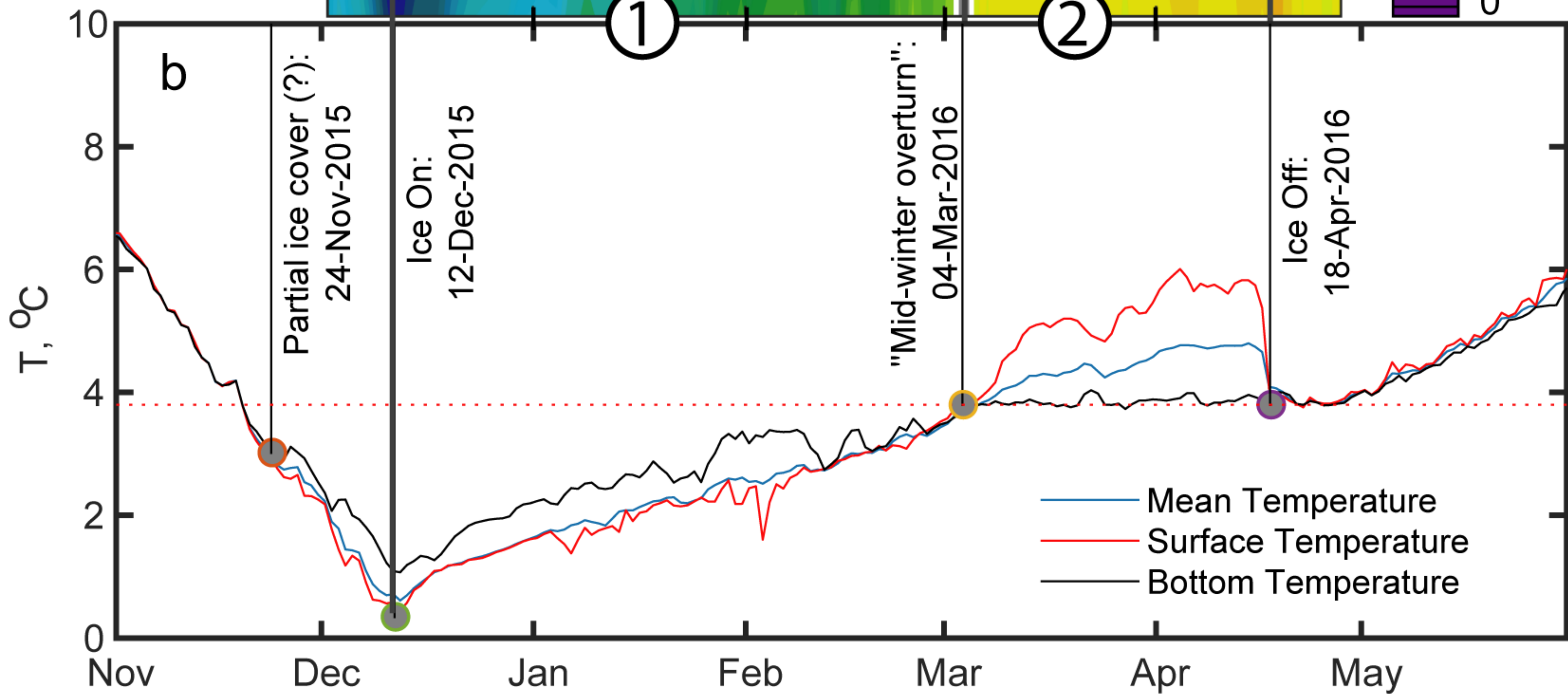
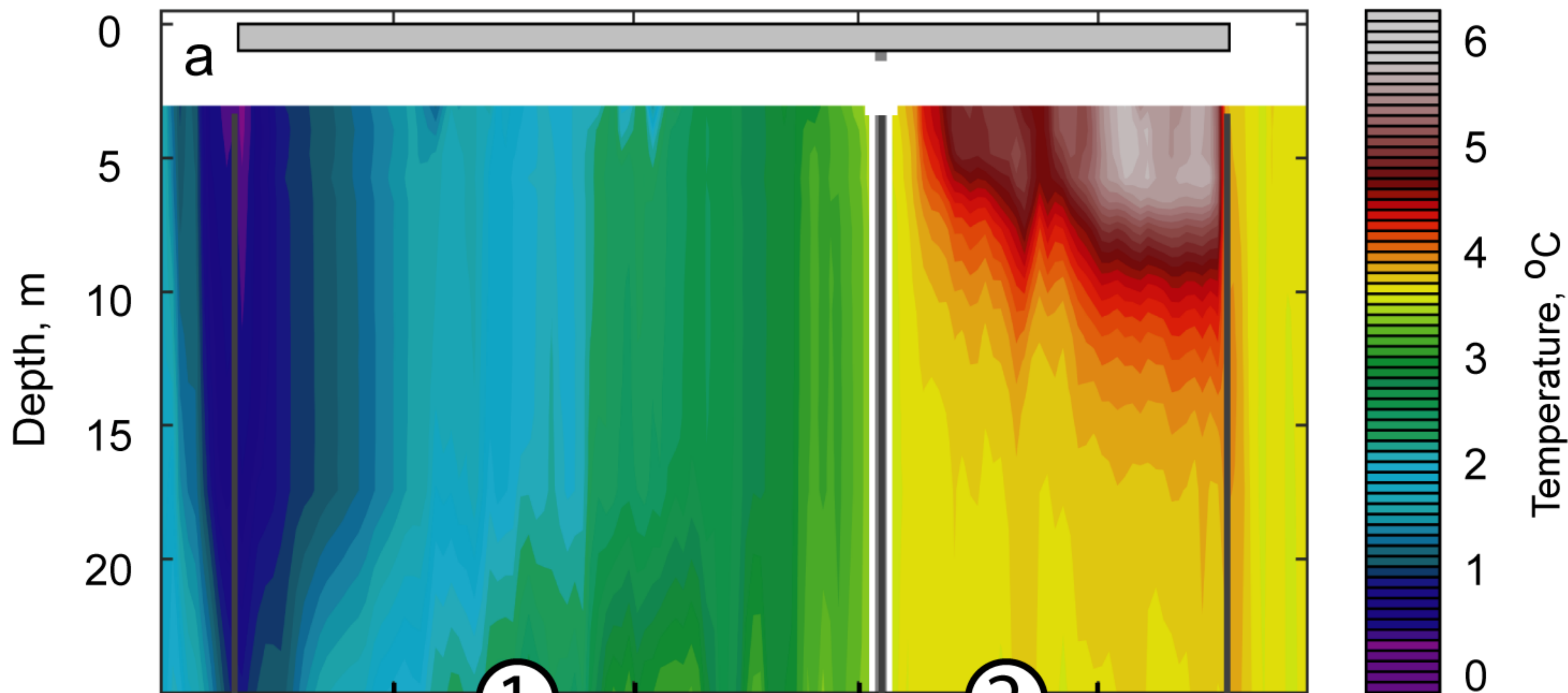


Figure 3.

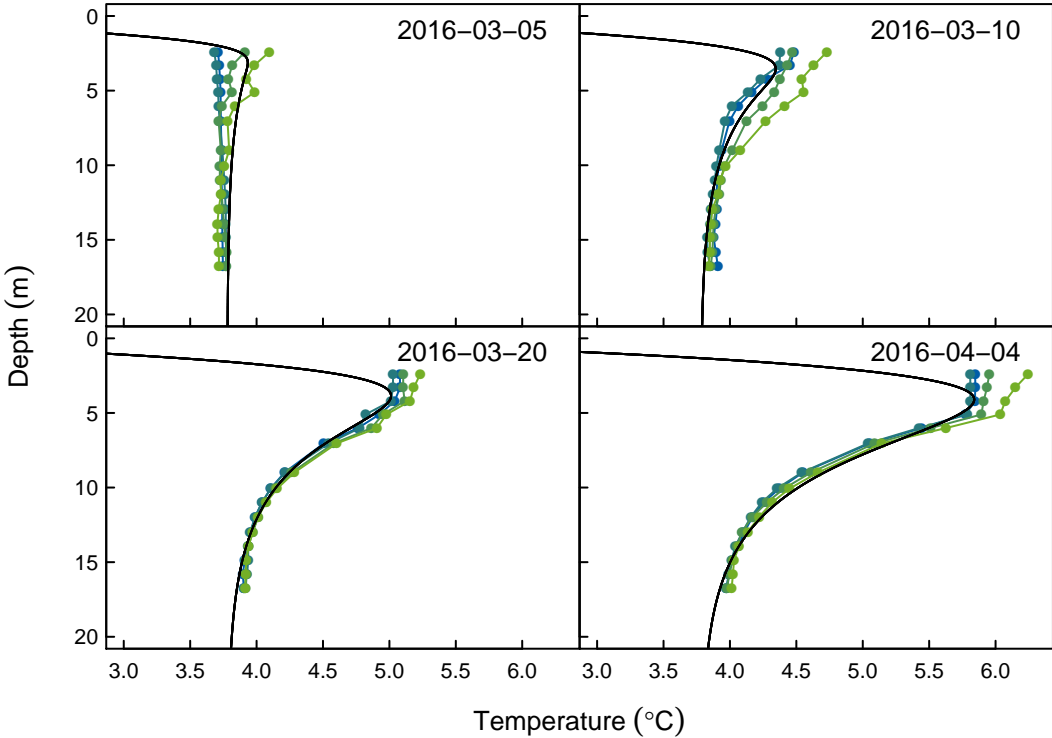


Figure 4.

